*Progress In Electromagnetics Research C, Vol. 134, 103–117, 2023*

# The Design of a Triple-Band H- and Dual C-Shaped Planar Dipole Antenna for a Drone Application

**Watcharaphon Naktong[1], Amnoiy Ruengwaree[2, *], Suwat Sakulchat[3, *], and Sommart Promput[4]**

**Abstract**—This paper presents the study of an H- and dual C-shaped planar dipole antenna by adding and etching technique for the triple-band of drone operating frequencies. Tuning the frequency range was performed to cover the VOR standard of 108–118 MHz, GS standard of 328.6–335.4 MHz, and the DME standard of 962–1,231 MHz. The antenna structure was fabricated on a PCB of FR4 with a dielectric constant ($\varepsilon_r$) of 4.4 and thickness ($h$) of 1.6 mm (material with low cost, compact size, and easy to use). The reflection coefficient ($S_{11}$) results of the simulation and measurement were in good agreement, which demonstrated the bandwidth frequencies of resonance frequency at 112 MHz (106–118 MHz), 331.50 MHz (323–401 MHz), and 1,087.50 MHz (920–1,301 MHz). The antenna gains were 1.73, 3.43, and 6.31 dBi, respectively, and the antenna radiation pattern was omnidirectional when it was used with $H$-plane. It was found in experiment that the proposed antenna could be installed in a drone with sending and receiving signals fittingly as desired. Furthermore, the proposed antenna is lightweight at just 0.4 kg, less than the original drone antenna (1.8 kg), and it does not require changing the antenna in each frequency range.

## 1. INTRODUCTION

Nowadays, drones are essential in human life because they substitute labor and expensive machinery, which use much energy. For example, using drones for security systems, agriculture to take care of cultivation and insecticide spray [1–4], surveying agricultural landscape areas that cannot be easily accessed [5, 6], surveying traffic in case of accidents or heavy traffic [7, 8], and for air traffic survey [9–11]. Drones are also used to inspect the exterior walls of buildings that humans are unable to inspect [12], for telecommunication systems [13–15], movie industry [16–18], etc. The antenna is the most important device that connects to the drone remote control. It is important for data transmission, flight control, and video and signal transmission of various data.

The drone antennas are designed to operate at a frequency band that covers the IEEE standard. For example, drones supporting IEEE 802.11b/g 2.45 GHz (2.40–2.48 GHz) are used for a general mission in agriculture for cultivation and insecticide spray, while the ones supporting IEEE 802.11a/n 5.80 GHz (5.15–5.75 GHz) are used for agriculture, farming landscape, and highway traffic [19–21]. Drones are also used in the frequency of VOR (Very High-Frequency Omnidirectional Range) standard frequency of 108–118 MHz [22], GS (Glide Slope) standard frequency of 328.6–335.4 MHz [23], and DME (Distance

*Received 15 March 2023, Accepted 8 June 2023, Scheduled 3 July 2023*

* Corresponding authors: Amnoiy Ruengwaree (amnoiy.r@en.rmutt.ac.th), Suwat Sakulchat (suwat.sa@rmutsb.ac.th).

[1] Department of Telecommunications Engineering, Faculty of Engineering and Technology, Rajamangala University of Technology Isan, Nakhon Ratchasima 30000, Thailand. [2] Department of Electronics and Telecommunication Engineering, Faculty of Engineering, Rajamangala University of Technology Thanyaburi, Pathum Thani 12110, Thailand. [3] Department of Electrical Engineering, Faculty of Engineering and Architecture, Rajamangala University of Technology Suvarnabhumi, Phranakhon Si Ayutthaya 13000, Thailand. [4] Department of Mechatronics and Robotics Engineering, School of Engineering and Innovation, Rajamangala University of Technology Tawan-ok, Chonburi 20110, Thailand.

Measuring Equipment) standard frequency of 962–1,231 MHz [24]. These frequencies are used for pre-flight inspection of planes, which measures the movement of the left and right sides, as well as the angle of departure for controlling drones.

Currently, available antennas mostly use a single frequency for a single antenna, as multiple frequencies in one or more antennas do not cover the operation frequency and are still expensive. If one needs to use it in any frequency, it must be switched to replace another antenna of the desired frequency.

Researchers have previously designed and developed antenna structures using various techniques to support the standard frequency. They designed a dual-band circular microstrip antenna operating in the 2.4 GHz and 5.2 GHz to enhance the bandwidth in those frequency ranges up to 4% and 7%, respectively. The circle radius of the thin-flexible Roger 5880 substrate was 76 mm, with five circular antennas placed on top. The first circular antenna of radius 23.25 mm was placed in the center. The second circular antennas with a radius of 22.90 mm were on the left and right, and there were also circular antennas with a radius of 10.19 mm, placed on top and bottom. They created a multiple-input multiple-output (MIMO) antenna with three antennas. Each of the three antennas is angled toward the other two, approximating the form of a triangle with a distance of 20 cm from the center of each element and placed it on an unmanned aerial vehicle (UAV) at the head and both wing positions [25]. A compact dual-band microstrip patch dipole-loop antenna for drone communications was designed. The antenna used an FR4 substrate that was 19 mm and 38 mm, which was used to attach to the drone on top. The loop antenna structure responded to the bandwidth of 2.3–2.4 GHz, while the dipole antenna structure responded to the bandwidth of 3.4–3.8 GHz and provided a bi-directional radiation pattern and a peak gain of 5 dBi [26]. A small and angle diversity monopole antenna was designed for small drones. The antenna was designed on a printed circuit board (PCB), shaped like a cross and provided on a $16 \times 16$ cm area, which responded to the bandwidth of 2.4 GHz and demonstrated that the radiation power distributed equally along all four arms with a gain of 4 dBi [27]. These included designing and fabricating a circular monopole antenna with a double I-shaped stub technique. That covered the ultra-wideband (UWB) (3.1–5.3 GHz) in IEEE standard 802.15.3a (3.1–10.6 GHz) and had an omnidirectional radiation pattern. The signal transmission test results were obtained at distances of $-200$ m by installing a sector antenna, with the best sending and receiving results being vertical-horizontal (VH) [28]. A study was conducted on the wind influence on a helical monopole antenna at wind speeds (1, 3, and 5 m/s) with $S_{11}$ and antenna gain compared. The experiments showed that 3 m/s and 5 m/s resulted in $S_{11}$ (at 9 MHz and 9.3 MHz), and antenna gain decreased by 20% and 60%, respectively [29]. A study was conducted on a bow-tie monopole antenna structure of $100 \times 100\,\text{mm}^2$, a thickness of 0.175 mm, printed on a circuit board (UTRALAM 350 HT, Rogers) with a dielectric of 3.12 and loss tangent of 0.002. The antenna had three structures whose operating frequency could be adjusted: conventional planer bow-tie antenna (CPBA), wrapped bow-tie antenna (WBA), and wrapped resistively loaded bow-tie antenna (WRLBA). The antenna structure was used by adjusting the CPBA to cover the frequency range of 2–10 GHz, the WBA to cover the frequency range of 4–10 GHz, and the WRLBA to cover the bandwidth range of 0.8–10 GHz [30]. A dual-band monopole antenna structure with two port connectors was used to reduce the complexity of an antenna structure built on FR4 with dimensions of $900 \times 600\,\text{mm}^2$, a thickness of 1.6 mm, and a dielectric constant of 4.4. The antenna structure with a basic rectangular shape showed a low frequency of 2.45 GHz at a bandwidth of 171 MHz and a high frequency of 5.80 GHz at a bandwidth of 643.6 MHz [31]. A Maxim antenna structure was used to verify drones which were not allowed to approach an airport operating in unlicensed ISM bands at 902–928 MHz. The operation test was examined at a distance of at least 15 m from the target. This antenna had a tracking error of 10.8 m [32]. However, the mentioned techniques very high-frequency omnidirectional range (VOR) with 108–118 MHz standards, GS, and DME with 962–1,231 MHz [25–27] are intriguing. They do not cover the required frequency range. The three frequency bands that measure left and correct movement frequencies and control the taking-off drone by distance angle all behave differently.

From the above review, this research focuses on developing a single antenna that can cover three frequencies: VOR (108–118 MHz), GS (328.6–335.4 MHz), and DME (962–1,231 MHz) to fit the standard operating frequency for monitoring plane take-off and landing in the airport. Slot antennas, microstrip antennas, waveguide antennas, and ring antennas all have a specific propagation direction

and are hard to tune, so dipole antennas have been selected for this research. The researchers decided on a dipole antenna structure with omnidirectional propagation covering the desired direction and facilitating tuning over the desired frequency. The prototype antenna structure is lighter than the original and not against the wind when the drone takes off. The antenna structure tuning process is described in Section 2. The test results and simulation results are explained in Section 3. The prototype dipole antenna experiment is explained in Section 4. The comparison on antenna efficiency is in Section 5, and Section 6 summarizes the research results.

## 2. ANTENNA DESIGN AND SIMULATION

The available original antenna structure, as shown in Figure 1, was developed for the structural design of the tri-band in a single antenna and used a VOR of 108–118 MHz for the low-frequency band, a GS of 328.6–335.4 MHz for the middle-frequency band, and a DME of 962–1,231 MHz for the high-frequency band. Many techniques have been studied, such as etching, adding stubs, drilling holes, and adding dielectric plates. If it was used in conjunction with a filter circuit or various electronic devices, it was found that the effect can be achieved within the desired operating frequency range. Furthermore, the apparent techniques that affected the antenna structure were adding stubs and etching, which had advantages in that the antenna structure was not complicated, easy to design, and low-cost. In this paper, the new antenna structure used a primary planar dipole antenna that was designed and fabricated on an FR4 substrate with a thickness ($h$) of 0.764 mm, dielectric ($\varepsilon_r$) of 4.4, copper thickness ($t$) of 0.017 mm, and conductivity of $5.8 \times 10^7$ S/m. The antenna structure design was 40 mm × 633 mm. The researchers used the dual I-shape etching technique [33, 34] and designed it on a copper plane with a dual rectangular stub [35, 36] to increase the bandwidth frequency to cover the standard frequency. This design was achieved by basic equation calculation to define parameters and adjust the antenna structure in four steps.

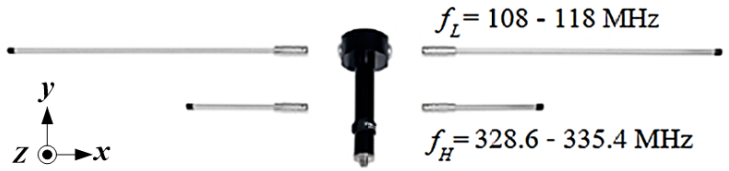


**Figure 1.** Original dipole antenna for a drone.

### 2.1. Determination of the Overall Size Antenna

The planar dipole antenna design was tested in real airport drones [37]. It was designed on an FR4 structure, which is lightweight, cheap, and had a good response for resonance frequency [38], with a dielectric constant ($\varepsilon_r$) of 4.4, thickness of the substrate ($h$) of 1.6 mm, conductivity of copper ($\sigma$) of $5.8 \times 10^7$ S/m, thickness of copper ($t$) of 0.035 mm, and loss tangent ($\delta$) of 0.015, as shown in Figure 2. This primary antenna design should be operated from the low-frequency to the high-frequency; the tuning process was initiated with the resonance frequency ($f_r$) of 113 MHz according to VOR standard (108–118 MHz) and was calculated as Equations (1)–(2) [37, 38].

Calculating the width $W = 633$ mm of the antenna from Equation (1).

$$W = \frac{0.5c}{f_r\sqrt{\varepsilon_r}} \tag{1}$$

Calculating the length $L = 40$ mm of the antenna from Equation (2)

$$L = \frac{0.015c}{f_r} \tag{2}$$

where

$c$ = velocity of the light ($3 \times 10^8$ ms)

$f_r$ = resonance frequency
$h$ = thickness of the substrate of FR4
$W$ = width of the antenna
$L$ = length of the antenna
$\lambda$ = wavelength
$\varepsilon_r$ = dielectric constant
$t$ = thickness of copper
$g$ = gap between antenna and ground

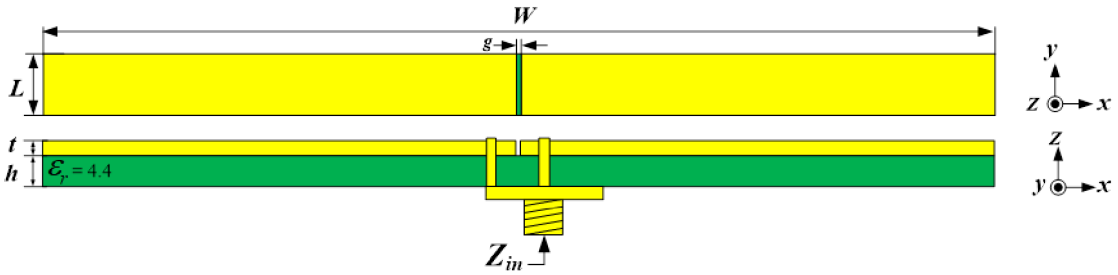


**Figure 2.** Antenna design fundamental model: basic planar dipole.

### 2.2. Simulation Results from Etching and Stub Enhancement

In the first step, the antenna parameters obtained from Equations (1)–(2) were used in the simulation to find the effect of the antenna frequency response characteristic achieved from the experiential method with the CST microwave suit. The simulation results demonstrated that the reflection coefficient was four frequency ranges below −10 dB, as shown in Figure 3. The low-frequency range was 7.16% (107–118 MHz) in area 1; the middle-frequency range was 3.08% (590–608 MHz) in area 2; the intermediate-frequency range was 7.24% (825–887 MHz) in area 3; and the high-frequency range was 7.14% (1,080–1,160 MHz) in area 4. The analysis showed that the antenna responded to the low-frequency band at 108–118 MHz but did not respond to the middle-frequency range of 328–336 MHz or the high-frequency range of 962–1,231 MHz.

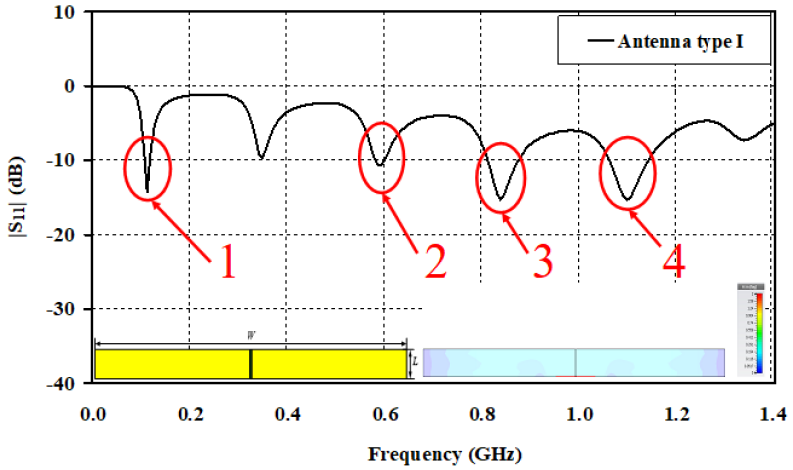


**Figure 3.** Reflection coefficient simulation result of the first-step tuning.

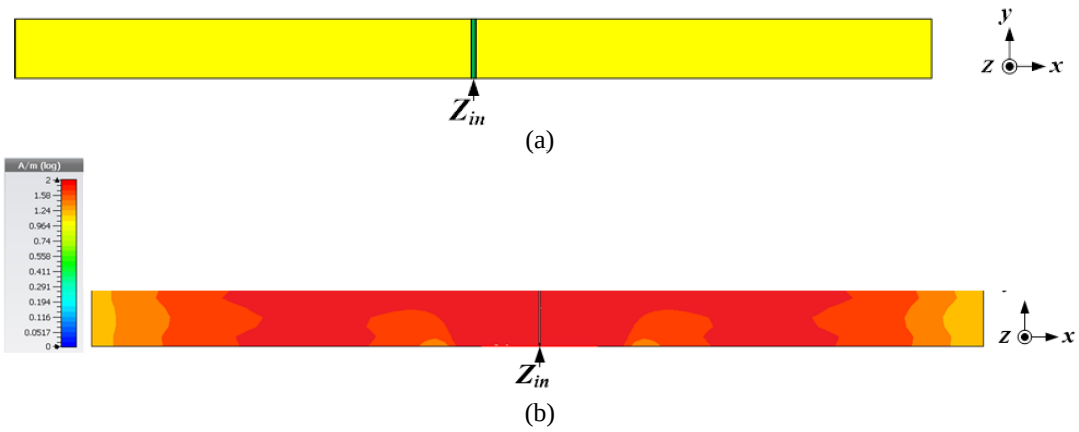


**Figure 4.** Planar dipole antenna configuration in the first step of tuning (a) physical of the antenna model and (b) the current distribution on the surface of the radiator.

The basic planar dipole antenna structure was modified in the second step by etching the copper plate [33, 34] to increase the middle-frequency range of GS (328.6–335.4 MHz). That was used to study the reflection coefficient and current density by observing the red intensity value on the antenna structure via the highest current density. The wavelength will affect the most usable frequency range if we tweak the antenna structure, as shown in Figure 4. The simulation results of the antenna structure showed a high current density on both arms from the feed point to the edge of the antenna. As a result, tuning was accomplished by etching the antenna with basic geometrical shapes [37] until the best shape was obtained, which was two horizontal I-shapes etched on copper plates at the bottom of both sides of the antenna, as shown in Figure 5(a), with a resonance frequency of 332 MHz.

As illustrated in Figure 5(a), a horizontal I-shaped slot ($W_1 \times L_1$) was etched into the copper plane to enhance the middle-frequency range for GS (328.6–335.4 MHz) which was calculated using Equations (3)–(4) [37, 38].

Calculating the width of the horizontal I-shape slot $W_1 = 133$ mm from Equation (3),

$$W_1 = \frac{0.5c}{f_r\sqrt{\varepsilon_r}}, \tag{3}$$

Calculating the length of the horizontal I-shape slot $L_1 = 18$ mm from Equation (4),

$$L_1 = \frac{0.015c}{f_r} \tag{4}$$

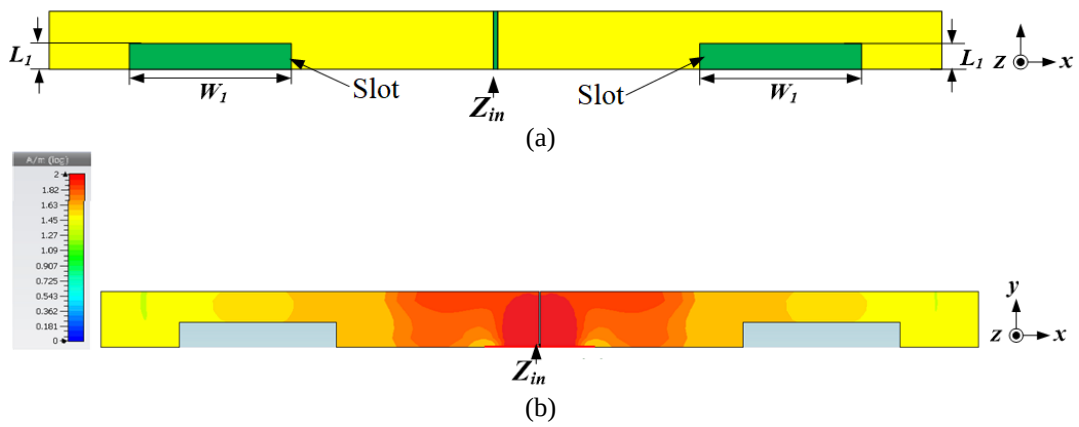


**Figure 5.** Planar dipole antenna configuration in the second step of tuning (a) the antenna with horizontal I-shape slot etching and (b) the current distribution on the surface of the radiator.

The parameters of the antenna could be calculated from Equations (3)–(4), with the initial parameters as follows: slot width value $W_1$ was fixed at 113 mm, and slot length $L_1$ was adjusted from 14, 16, 18, 20, and 22 mm with 18 mm as the optimal value. The reflection coefficient was below −10 dB with five frequency ranges: 104–115 MHz (10.04%), 323–340 MHz (5.12%), 573–594 MHz (3.60%), 789–857 MHz (8.26%), and 1,013–1,179 MHz (15.14%), which responded to the low-frequency 108–118 MHz at the area $A_1$ and the middle-frequency 328–336 MHz at the area $A_2$, but still did not respond to the high-frequency 962–1,231 MHz, as required at the area $A_3$, as shown in Figure 6.

In the third step, the antenna was improved with an etching technique on the copper plate above the feed point [37] to increase the frequency range for DME (962–1,231 MHz). That is based on the resonance coefficient and current density from the antenna structure simulation which found high current density at the antenna center near the feed point (Figure 5(b)). Etching was performed for tuning by selecting basic geometric shapes, such as square, rectangle, circle, and triangle [37]. The optimal slot shape was the triangle that was placed to the left and right of the center point of the antenna as shown in Figure 7(a), which enhanced the high-frequency range DME (962–1,231 MHz) and could be calculated from Equations (5)–(6) [37, 38], as shown in Figure 7(b).

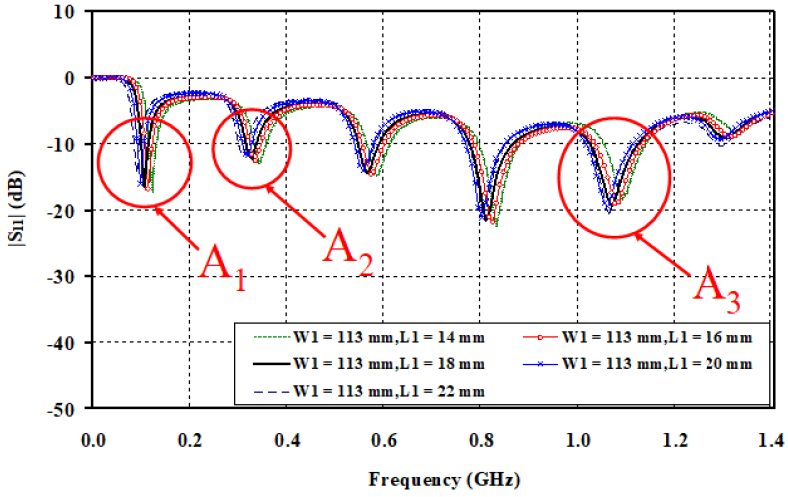


**Figure 6.** Simulation result of the reflection coefficient in the second step tuning.

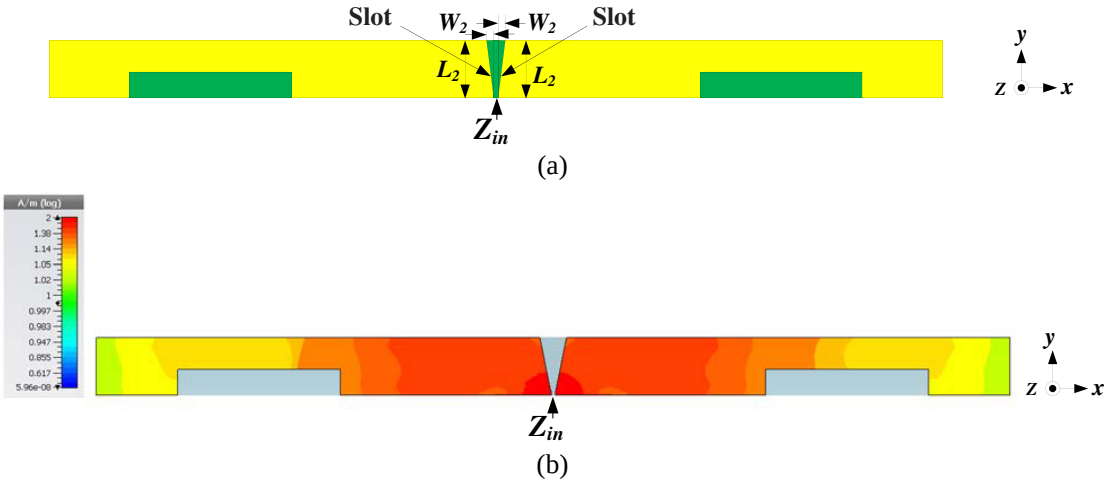


**Figure 7.** Planar dipole antenna configuration in the third step of tuning (a) the antenna with horizontal I- and triangle-shape slot etching and (b) the current distribution on the surface of the radiator.

Calculating the width of the triangle etching $W_2 = 4$ mm from Equation (5),

$$W_2 = \frac{0.5c}{f_r\sqrt{\varepsilon_r}}, \tag{5}$$

Calculating the length of the triangle etching $L_2 = 40$ mm from Equation (6),

$$L_2 = \frac{0.015c}{f_r} \tag{6}$$

The resonance frequency at the high-frequency range was 1,097 MHz, calculated as in Equations (5)–(6). The basic parameters were as follows: length constant $L_2$ of 40 mm and width $W_2$ by adjusting values of 2, 3, 4, 5, and 6 mm with 4 mm as the optimal value. The reflection coefficient was below −10 dB at six frequency ranges: 10.04% (104–118 MHz), 4.82% (324–340 MHz), 3.97% (568–591 MHz), 7.52% (780–841 MHz), 23.36% (979–1,238 MHz), and 6.44% (1,321–1,409 MHz), which only responded to the low-frequency of 108–118 MHz and middle frequency of 328–336 MHz. However, this still did not respond to the high frequency of 962–1,231 MHz at the area $B$ as desired. Some frequency ranges were also not desirable, such as the frequency range of 3.97% (568–591 MHz), 7.52% (780–841 MHz), and 6.44% (1,321–1,409 MHz) in the area $C$, as shown in Figure 8.

Finally, the dual stubs were added to both arms of the proposed planar dipole antenna to improve high-frequency response and precise undesired frequency [38] from the previous design step (area $C$, as shown in Figure 8). The optimal geometric shape for the stub was rectangular, as shown in Figure 9.

The dual stubs were added to the antenna also to cut off the inactive frequency range which could be calculated from Equations (7)–(9) [38]. The resonance frequency at the high-frequency range of 1,097 MHz was calculated by Equations (7)–(9) with a fixed $W_3$ amplitude constant of 47 mm and adjusted length of $L_3$ as follows: 124, 134, 144, 154, and 164 mm.

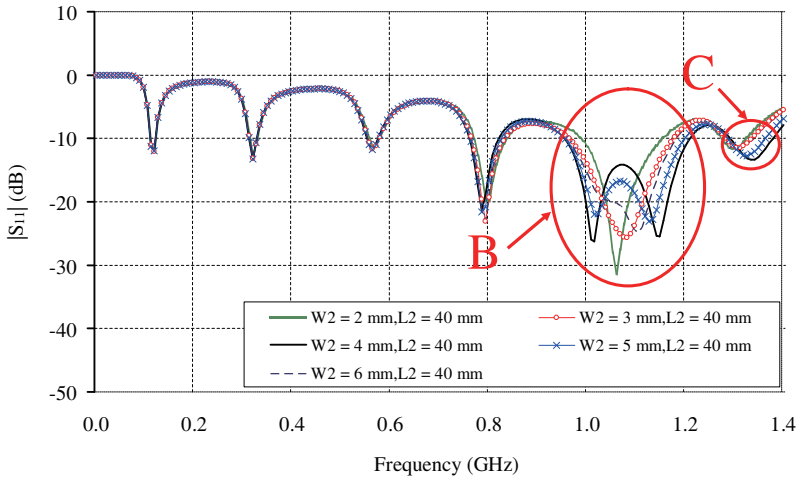


**Figure 8.** Simulation results of the reflection coefficient in the third step tuning.

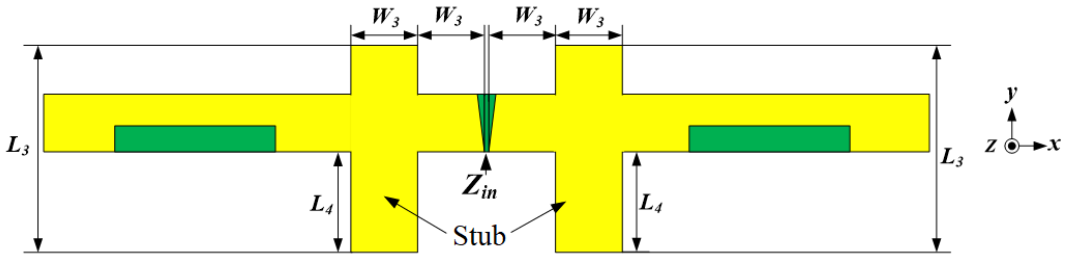


**Figure 9.** Planar dipole antenna configuration in the final step of tuning.

Calculating the width of the rectangular stub $W_3 = 47\,\text{mm}$ from Equation (7),

$$W_3 = \frac{0.5c}{f_r\sqrt{\varepsilon_r}}, \tag{7}$$

Calculating the width of the rectangular stub $L_3 = 144\,\text{mm}$ from Equation (8),

$$L_3 = \frac{0.015c}{f_r} \tag{8}$$

Calculating the width of the rectangular stub $L_4 = 70\,\text{mm}$ from Equation (9),

$$L_4 = \frac{0.007c}{f_r} \tag{9}$$

The simulation result revealed that the optimum length $L_3$ was 144 mm with the reflection coefficient below −10 dB at three frequency ranges: 11.5% (106–119 MHz), 9.05% (317–347 MHz), and 40.15% (936–1,418 MHz) responding to the low-frequency of 108–118 MHz, middle-frequency of 328–336 MHz, and high-frequency of 962–1,231 MHz, according to the required standards, as shown in Figure 10.

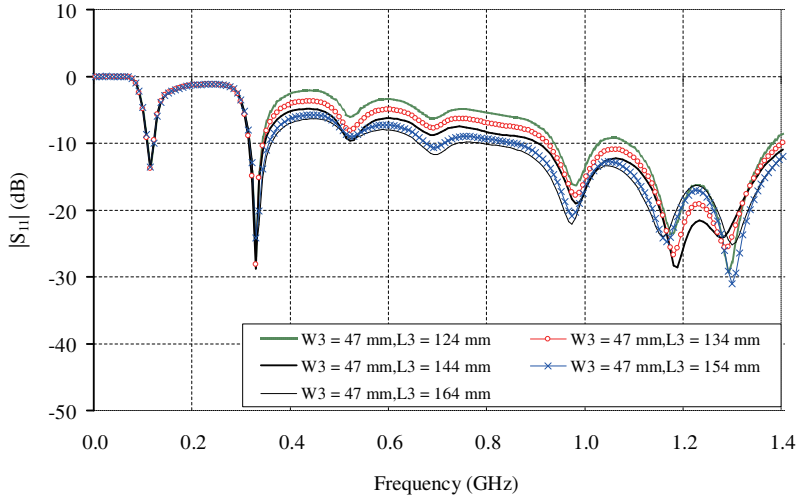


**Figure 10.** Simulation results of the reflection coefficient in the final step tuning.

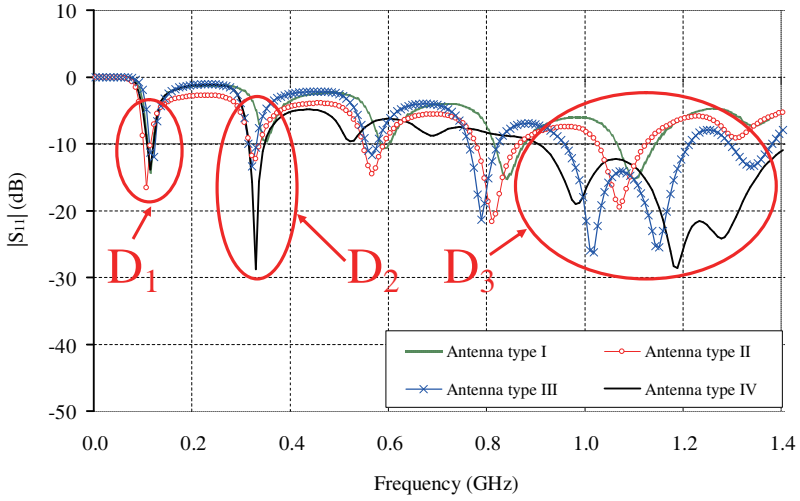


**Figure 11.** Comparison of reflection coefficient simulation results in all-step tuning.

The proposed planar dipole antenna was designed by adjusting the structure in four steps, with the best operating frequency range obtained by comparing the simulation results of the reflection coefficient of the four antennas, as shown in Figure 11. The stub tuning with a rectangular antenna positively influenced the frequency range required for the low frequency of the VOR band (108–118 MHz) at area $D_1$, the middle frequency of the GS band (328.6–335.4 MHz) at area $D_2$, and the high-frequency of DME band (962–1,231 MHz) at area $D_3$. The prototype planar dipole antenna structure parameters are shown in Figure 12 and Table 1.

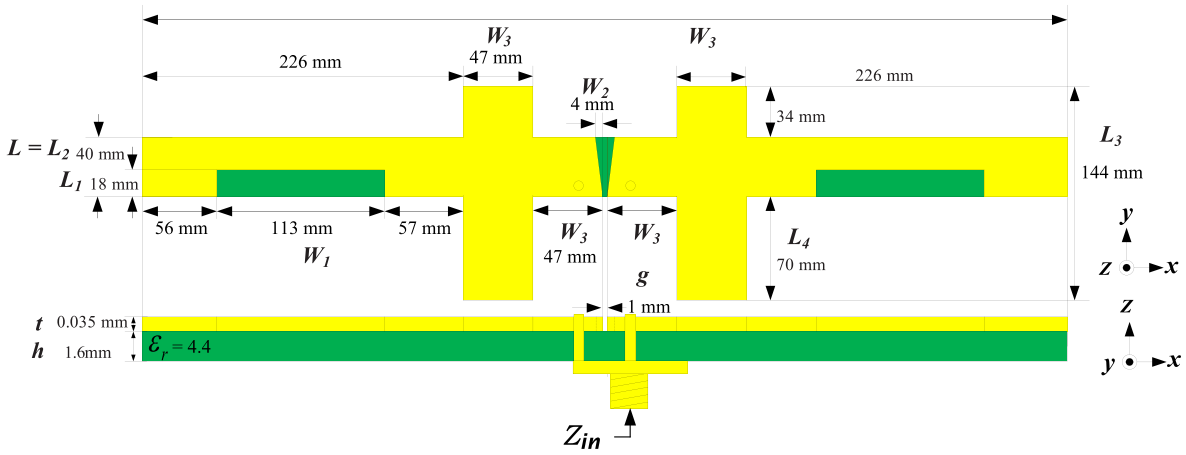


**Figure 12.** Proposed planar dipole antenna structure.

**Table 1.** Optimized parameters of the proposed planar dipole antenna.

| Parameters | Size (mm) |
|---|---|
| $W$: width of the dipole antenna | 633 |
| $W_1$: width of the horizontal I-shape slot | 113 |
| $W_2$: width of the triangle slot | 4 |
| $W_3$: width of the rectangular stub | 47 |
| $L$: length of the dipole antenna | 40 |
| $L_1$: length of the horizontal I-shape slot | 18 |
| $L_2$: length of the triangle slot | 40 |
| $L_3$: length of the rectangular stub | 144 |
| $L_4$: length of the rectangular stub | 34 |
| $g$: width of the gap | 0.3 |
| $t$: thickness of the antenna | 0.035 |
| $h$: thickness of the substrate | 1.6 |

## 3. ANTENNA MEASUREMENT

The proposed planar dipole antenna was fabricated using the parameters in Table 1, as shown in Figure 13(a). Network Analyzer (Agilent: E5071C), as shown in Figure 13(b), was used to measure antenna characteristics such as the reflection coefficient, voltage standing wave ratio (VSWR), input impedance ($Z_{in}$), antenna gain, and radiation pattern for comparison with the simulation results. The measurement results indicated that the reflection coefficient for the lower-frequency range was −16.85 dB (106–118 MHz), −15.63 dB (325–338 MHz) for the middle-frequency range, and −25.05 dB


(a) (b)

**Figure 13.** Photograph of proposed planar dipole antenna and equipment, (a) the prototype antenna was fabricated using the parameters in Table 1 and (b) Network Analyzer (Agilent: E5071C) was used to measure antenna characteristics.

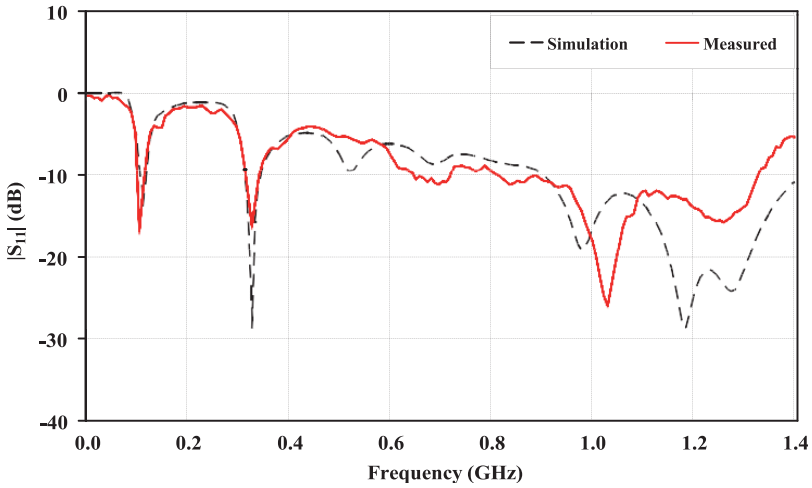


**Figure 14.** Comparison of reflection coefficient between simulation and measurement results.

(875–1,300 MHz) for the higher-frequency range as shown in Figure 14. The comparison of the reflection coefficients of the simulation and measurement results revealed that the lower and middle-frequency ranges were similar, and the higher frequency range was slightly different. This slight difference in the higher frequency range was due to the poor quality of connecting the SMA connector to the antenna. The VSWR was 1.79 : 1, 1.56 : 1, and 1.81 : 1, respectively. The input impedance was $40.55 - j23.49\,\Omega$, $80.43 + j0.38\,\Omega$, and $38.99 + j25.00\,\Omega$, respectively, and the antenna gain was 1.73 dB, 3.43 dB, and 6.31 dB, respectively, as shown in Table 2. The radiation pattern was bidirectional at the $E$-plane and omnidirectional at the $H$-plane. The comparison of characteristics of the antenna simulation results agreed well with the measurement results, as shown in Figures 15–17.

**Table 2.** The measured characteristic results of the proposed antenna.

| Antenna parameters | $f_r$ MHz | $S_{11}$ (dB) | $f_c$ (MHz) | BW MHz | Bandwidth (%) | VSWR | $Z_{in}$ ($\Omega$) | Gain (dBi) |
|---|---|---|---|---|---|---|---|---|
| Measured | 111 | −16.85 | 112 | 106–118 | 10.70 | 1.79 : 1 | $44.35 + j29.63$ | 1.73 |
| | 332 | −15.63 | 331.50 | 325–338 | 3.92 | 1.56 : 1 | $80.43 + j0.38$ | 3.43 |
| | 1,016 | −25.05 | 1,087.50 | 875–1,300 | 39.08 | 1.81 : 1 | $38.99 + j25.00$ | 6.31 |

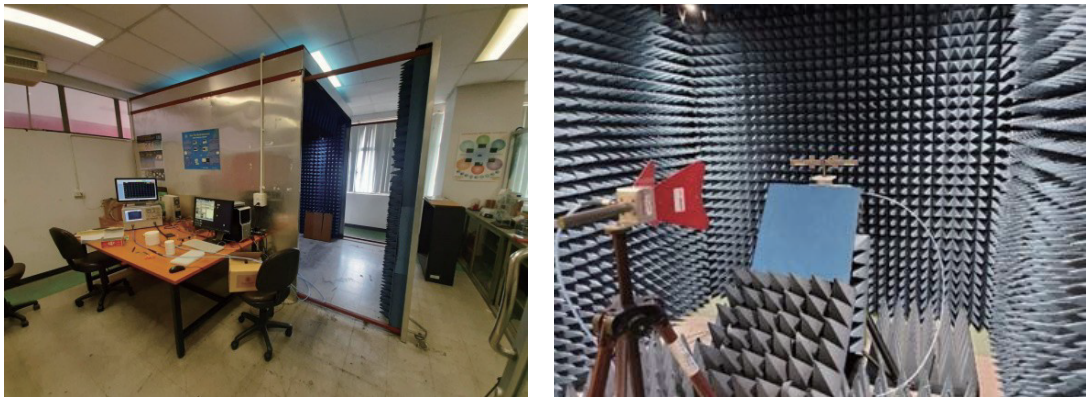

(a) (b)

**Figure 15.** Providing the ability to measure radiation patterns, (a) chamber area with equipment and (b) preparing the antenna prototype in the chamber.

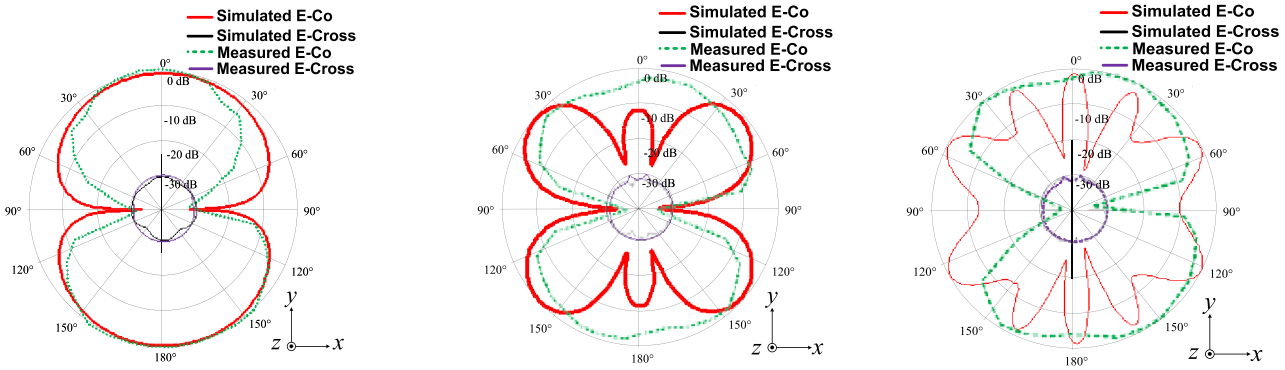


(a) (b) (c)

**Figure 16.** Comparison of measured and simulated results of $E$-plane radiation patterns of the proposed antenna (a) at 113 MHz, (b) at 332 MHz and (c) at 1,096.5 MHz.

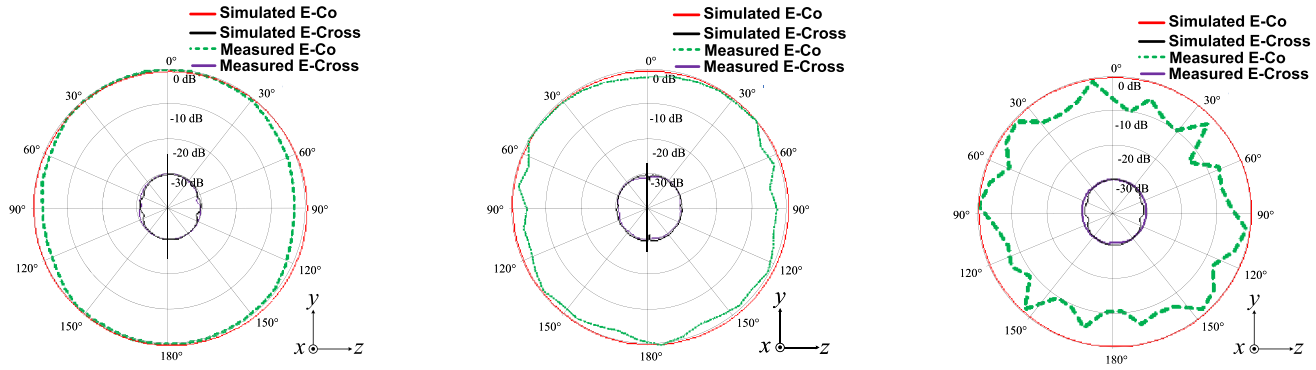


(a) (b) (c)

**Figure 17.** Comparison of measured and simulated results of $H$-plane radiation patterns of the proposed antenna (a) at 113 MHz, (b) at 332 MHz and (c) at 1,096.5 MHz.

## 4. EXPERIMENTAL ANTENNA

The prototype antenna was connected to a drone on $H$-plane for the experimental real-life situation as shown in Figure 18 (at the low-frequency range of 113 MHz, middle-frequency range of 332 MHz, and

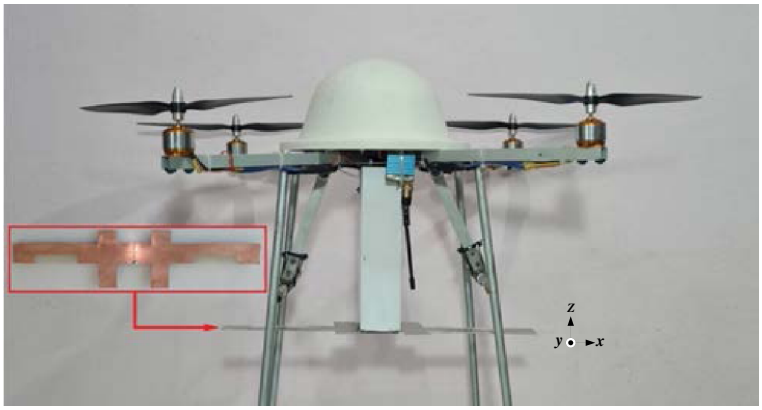


**Figure 18.** Mounting the proposed antenna to a drone on an $H$-plane for the experiment.

high-frequency range of 1,096.5 MHz). The proposed antenna was compatible with the drone, and its weight was reduced from 1.5 kg to 0.4 kg, eliminating the need to change the antenna in each frequency range. The wind load in this experiment was controlled at 1–5 m/s [29], which did not affect the frequency range or antenna gain.

## 5. DISCUSSION

The proposed antenna was compared with previous research such as [28]: a circular monopole antenna on an FR4 substrate that covered the UWB (3.1–5.3 GHz) and was obtained at distances of −200 m; [29]: a helical antenna mounted on drones of high frequency (HF) band supporting 9.0–9.3 MHz; [30]: a bow-tie monopole antenna structure on a Rogers substrate adjusted with three structures (CPBA, WBA, and WRLBA) covering the frequency of 2–10 GHz, 4–10 GHz, and 0.8–10 GHz, respectively; [31]: a dual-band monopole antenna on an FR4 substrate fabricated for 2.45 GHz and 5.80 GHz; and [32]: a Maxim antenna structure designed for operating in ISM bands at 902–928 MHz.

This comparison focused on antenna efficiency obtained from the frequency range, dimensions of the antenna, and the antenna gain. The antenna structure was designed for the drone with three frequencies: VOR standard 108–118 MHz, GS standard 328.6–335.4 MHz, and DME standard 962–1,231 MHz, which was better than [38], as shown in Table 3.

**Table 3.** Performance comparison of the proposed antenna with different types.

| Reference | Frequency range (MHz) | Substrate | Antenna size ($mm^3$) | Gain (dBi) |
|---|---|---|---|---|
| [28] | 2,200–5,300 | FR4 | - | - |
| [29] | 9 | Wire | $1500 \times 1$ | 4.5 |
| [30] | 100–10,000 | Rogers | $100 \times 100 \times 0.175$ | - |
| [31] | 2,400/5,800 | FR4 | $9 \times 6 \times 1.6$ | 0.33/0.41 |
| [32] | 902–928 | Wire | $117 \times 440 \times 1$ | - |
| [38] | 107–125/328–352 | FR4 | $700 \times 40 \times 1.6$ | 2.13/3.21 |
| Proposed antenna | 106–118/325–338/875–1,300 | FR4 | $633 \times 144 \times 1.6$ | 1.73/3.43/6.31 |

## 6. CONCLUSION

The proposed dipole antenna structure was designed and fabricated by etching an I-shaped and triangle shaped slot and adding a rectangular stub on both arms of the patch dipole antenna. This antenna could support three operating frequency ranges: low-frequency 106–118 MHz, middle-frequency

325–338 MHz, and high-frequency 875–1,300 MHz, which covered VOR (Very High-Frequency Omni-Directional Range) standard 108–118 MHz, GS (Glide Slope) standard 328.6–335.4 MHz, and DME (Distance Measuring Equipment) standard 962–1,231 MHz as desired. The radiation pattern with the $H$-plane was omnidirectional; the average antenna gains at low, middle, and high frequencies were 1.73 dB, 3.43 dB, and 6.31 dB, respectively. The experiment showed that the proposed planar dipole antenna could be installed on the drone and used to receive and transmit signals correctly as desired. Furthermore, this antenna weighed just 0.4 kg, lighter than the original antenna (1.8 kg), and functioned without changing the antenna with every frequency range. Although FR4 substrate is widely available and cheap, it still cannot respond to high frequency very well. In the future, the researchers will study other materials such as Rogers, RT/duroid to be used to fabricate antenna structures that can respond to higher operating frequencies.

## ACKNOWLEDGMENT

The authors would like to thank the Department of Telecommunications Engineering, Faculty of Engineering and Technology, Rajamangala University of Technology Isan for providing equipment and research funding. The authors also gratefully acknowledge the Department of Electronics and Telecommunication Engineering, Faculty of Engineering, Rajamangala University of Technology Thanyaburi, Pathum Thani, for supporting this work with the simulation CST software and the Department of Electrical Engineering, Faculty of Engineering and Architecture, Rajamangala University of Technology Suvarnabhumi, Phranakhon Si Ayutthaya, for supporting the experimental site.

## REFERENCES

1. Yanmaz, E., S. Yahyanejad, B. Rinner, H. Hellwagner, and C. Bettstetter, "Drone networks: Communications, coordination, and sensing," *Ad Hoc Networks*, Vol. 68, 1–15, 2018.
2. Belyaev, E. and S. Forchhammer, "An efficient storage of infrared video of drone inspections via iterative aerial map construction," *IEEE Signal Processing Letters*, Vol. 26, No. 8, 1157–1161, 2019.
3. Ahirwar, S., R. Swarnkar, S. Bhukya, and G. Namwade, "Application of drone in agriculture," *International Journal of Current Microbiology and Applied Sciences*, Vol. 8, No. 1, 2500–2505, 2019.
4. Puri, V., A. Nayyar, and L. Raja, "Agriculture drones: A modern breakthrough in precision agriculture," *Journal of Statistics and Management Systems*, Vol. 20, No. 4, 507–518, 2017.
5. Besada, J. A., L. Bergesio, I. Campaña, D. Vaquero-Melchor, J. López-Araquistain, M. Bernardos, and J. R. Casar, "Drone mission definition and implementation for automated infrastructure inspection using airborne sensors," *Sensors*, Vol. 18, No. 4, 1170, 2018.
6. Bendig, J., A. Bolten, S. Bennertz, J. Broscheit, S. Eichfuss, and G. Bareth, "Estimating biomass of barley using crop surface models (CSMs) derived from UAV-based RGB imaging," *Remote Sensing*, Vol. 6, No. 11, 10395–10412, 2014.
7. Colomina, I. and P. Molina, "Unmanned aerial systems for photogrammetry and remote sensing: A review," *ISPRS Journal of Photogrammetry and Remote Sensing*, Vol. 92, 79–97, 2014.
8. Restrepo, D., "Naked soldiers, naked terrorists, and the justifiability of drone warfare," *Social Theory and Practice*, 103–126, 2019.
9. Wild, G., J. Murray, and G. Baxter, "Exploring civil drone accidents and incidents to help prevent potential air disasters," *Aerospace*, Vol. 3, No. 3, 22, 2016.
10. Brown, A. S., "The drone warriors," *Mechanical Engineering*, Vol. 132, No. 1, 22–27, 2010.
11. Henriksen, A. and J. Ringsmose, "Drone warfare and morality in riskless war," *Global Affairs*, Vol. 1, No. 3, 285–291, 2015.
12. Burke, P. J., "Small unmanned aircraft systems (SUAS) and manned traffi near John Wayne Airport (KSNA) spot check of the SUAS facility map: Towards a new paradigm for drone safety near airports," *Drones*, Vol. 3, No. 4, 84, 2019.

13. Yu, J. J., D. W. Kim, E. J. Lee, and S. W. Son, "Determining the optimal number of ground control points for varying study sites through accuracy evaluation of unmanned aerial system-based 3D point clouds and digital surface models," *Drones*, Vol. 4, No. 3, 49, 2020.
14. Strumberger, I., N. Bacanin, S. Tomic, M. Beko, and M. Tuba, "Static drone placement by elephant herding optimization algorithm," *2017 25th Telecommunication Forum (Telfor)*, 1–4, IEEE, November 2017.
15. Cauchard, J. R., A. Tamkin, C. Y. Wang, L. Vink, M. Park, T. Fang, and J. A. Landay, "Drone. IO: A gestural and visual interface for human-drone interaction," *2019 14th ACM/IEEE International Conference on Human-Robot Interaction (HRI)*, 153–162, IEEE, March 2019.
16. Grubesic, T. H. and J. R. Nelson, "Drone futures," *UAVs and Urban Spatial Analysis*, 189–200, Springer, Cham, 2020.
17. Coluccia, A., A. Fascista, A. Schumann, L. Sommer, A. Dimou, D. Zarpalas, and I. Mantegh, "Drone-vs-bird detection challenge at IEEE AVSS2021," *2021 17th IEEE International Conference on Advanced Video and Signal Based Surveillance (AVSS)*, 1–8, IEEE, November 2021.
18. Kalantari, E., M. Z. Shakir, H. Yanikomeroglu, and A. Yongacoglu, "Backhaul-aware robust 3D drone placement in 5G+ wireless networks," *2017 IEEE International Conference on Communications Workshops (ICC Workshops)*, 109–114, IEEE, May 2017.
19. Katila, C. J., A. Di Gianni, C. Buratti, and R. Verdone, "Routing protocols for video surveillance drones in IEEE 802.11s wireless mesh networks," *2017 European Conference on Networks and Communications (EuCNC)*, 1–5, IEEE, June 2017.
20. Berzinis, R., A. Carroll, D. Cronwell, L. Ford, H. Fravel, C. Hedman, and N. Parker, *Environmental Assessment: Relocation and Construction of the Panama City-Bay County International Airport (PFN) Doppler Very High Frequency Omni-directional Radio Range Tactical Air Navigation Aid (VORTAC) to Tyndall Air Force Base (TAFB)*, PBS and J Panama City Beach, FL, 2010.
21. Horapong, K., D. Chandrucka, N. Montree, and P. Buaon, "Design and use of "Drone" to support the radio navigation aids flight inspection," *2017 IEEE/AIAA 36th Digital Avionics Systems Conference (DASC)*, 1–6, IEEE, September 2017.
22. Hu, Y. H. and X. L. Zhang, "A new method of distance measuring based on frame synchronization code for airborne target drone," *2006 IEEE International Symposium on Industrial Electronics*, Vol. 4, 2710–2713, IEEE, July 2006.
23. Chen, J., D. Raye, W. Khawaja, P. Sinha, and I. Guvenc, "Impact of 3D UWB antenna radiation pattern on air-to-ground drone connectivity," *2018 IEEE 88th Vehicular Technology Conference (VTC-Fall)*, 1–5, IEEE, August 2018.
24. Kawabata, K. and A. R. A. I. Hiroyuki, "Wind influence of air wire antenna suspended from drone," *2018 International Symposium on Antennas and Propagation (ISAP)*, 1–2, IEEE, October 2018.
25. Akhter, Z., R. M. Bilal, and A. Shamim, "A dual mode, thin and wideband MIMO antenna system for seamless integration on UAV," *IEEE Open Journal of Antennas and Propagation*, Vol. 2, 991–1000, 2021.
26. Celik, F. T. and K. Karacuhha, "Dual-band microtrip Quasi-Yagi antenna design for free band and 5G mobile communication," *2018 XXIIIrd International Seminar/Workshop on Direct and Inverse Problems of Electromagnetic and Acoustic Wave Theory (DIPED)*, 189–192, IEEE, September 2018.
27. Seo, Y., M. Jeon, J. Cho, Y. Lee, J. Jang, C. Lee, and S. Kahng, "A small and angle-diversity antenna mountable for the small drone," *2021 International Conference on Information and Communication Technology Convergence (ICTC)*, 994–996, IEEE, October 2021.
28. Lee, D., G. Shaker, and W. Melek, "Flexible antenna on drone arms for near-field sensing applications," *2018 18th International Symposium on Antenna Technology and Applied Electromagnetics (ANTEM)*, 1–2, IEEE, August 2018.
29. Nathaniel, E. B., H. Wijanto, and E. Edwar, "Perancangan dan realisasi antenna mikrostrip celah pita-ganda 2,4 GHz dan 5,8 GHz untuk drone," *Proceedings of Engineering*, Vol. 6, No. 2, 2019.
30. Dressel, L. and M. J. Kochenderfer, "Hunting drones with other drones: Tracking a moving radio target," *2019 International Conference on Robotics and Automation (ICRA)*, 1905–1912, IEEE, May 2019.

31. Naktong, W., S. Kronsing, and A. Ruengwaree, "The bandwidth enhancement of rectangular slot antenna with H and T-shaped slot tuning for ultrawideband applications," *2014 11th International Conference on Electrical Engineering/Electronics, Computer, Telecommunications and Information Technology (ECTI-CON)*, 1–4, IEEE, May 2014.
32. Naktong, W., B. Kaewchan, A. Namsang, and A. Ruengwaree, "Bidirectional antenna on flambeau-shape," *International Symposium on Antennas Propagation*, November 2010.
33. Ruengwaree, A., A. Innok, and W. Naktong, "The bandwidth enhancement of rectangular slot antenna with L-shaped and double I-shaped stub tuning for WLAN/WiMAX applications," *2015 12th International Conference on Electrical Engineering/Electronics, Computer, Telecommunications and Information Technology (ECTI-CON)*, 1–4, IEEE, June 2015.
34. Chanramrd, S., W. Naktong, P. Thongbor, S. Sakulchat, A. Ruengwaree, and A. Namsang, "The structure tuning of plugs-shaped monopole antenna for wireless communication applications," *2017 International Symposium on Antennas and Propagation (ISAP)*, 1–2, IEEE, October 2017.
35. Komsing, S., N. Fhafhiem, A. Innok, and A. Ruengwaree, "Design of wide-band dipole antenna for digital TV broadcasting application," *2018 International Electrical Engineering Congress (iEECON)*, 1–4, IEEE, March 2018.
36. Ruengwaree, A., W. Naktong, and A. Namsang, "A TE-shaped monopole antenna with semicircle etching technique on ground plane for UWB applications," *2013 Proceedings of the International Symposium on Antennas & Propagation*, Vol. 1, 95–98, IEEE, October 2013.
37. Balanis, C. A., *Antenna Theory: Analysis and Design*, John Wiley & Sons, 2015.
38. Naktong, W., S. Sakulchat, A. Ruengwaree, A. Namsang, and L. Ruengyote, "Study of a dipole antenna tuned by triangle-shaped slot for Drone," *The 10th Engineering, Science, Technology and Architecture Conference 2019 (ESTACON 2019)*, 96–99, Nakhon Ratchasima, Thailand, 2019.